Diffusion Tractography and Graph Theory Analysis Reveal the Disrupted Rich-Club Organization of White Matter Structural Networks in Early Tourette Syndrome Children

Hongwei Wen[1,2a], Yue Liu[4a], Shengpei Wang[1,2], Jishui Zhang[5], Yun Peng[4*], Huiguang He[1,2,3*]
[1] Research Center for Brain-inspired Intelligence, Institute of Automation, Chinese Academy of Sciences, Beijing, China
[2] University of Chinese Academy of Sciences, Beijing, China
[3] Center for Excellence in Brain Science and Intelligence Technology, Chinese Academy of Sciences, Beijing, China
[4] Department of Radiology, Beijing Children's Hospital, Capital Medical University, Beijing, China
[5] Department of Neurology, Beijing Children's Hospital, Capital Medical University, Beijing, China

ABSTRACT

Tourette syndrome (TS) is a childhood-onset neurobehavioral disorder. At present, the topological disruptions of the whole brain white matter (WM) structural networks remain poorly understood in TS children. Considering the unique position of the topologically central role of densely interconnected brain hubs, namely the rich club regions, therefore, we aimed to investigate whether the rich club regions and their related connections would be particularly vulnerable in early TS children. In our study, we used diffusion tractography and graph theoretical analyses to explore the rich club structures in 44 TS children and 48 healthy children. The structural networks of TS children exhibited significantly increased normalized rich club coefficient, suggesting that TS is characterized by increased structural integrity of this centrally embedded rich club backbone, potentially resulting in increased global communication capacity. In addition, TS children showed a reorganization of rich club regions, as well as significantly increased density and decreased number in feeder connections. Furthermore, the increased rich club coefficients and feeder connections density of TS children were significantly positively correlated to tic severity, indicating that TS may be characterized by a selective alteration of the structural connectivity of the rich club regions, tending to have higher bridging with non-rich club regions, which may increase the integration among tic-related brain circuits with more excitability but less inhibition for information exchanges between highly centered brain regions and peripheral areas. In all, our results suggest the disrupted rich club organization in early TS children and provide structural insights into the brain networks.

Keywords: Tourette syndrome, Diffusion tensor imaging, Diffusion tractography, Graph theoretical analysis, Rich club

1. INTRODUCTION

Tourette syndrome (TS) is a childhood-onset neurobehavioral disorder characterized by the presence of multiple motor and vocal tics. The typical age of onset is between 5–7 years with the worst tic severity for most patients falls between age7-15 year [1]. Affected individuals are at increased risk for the development of various comorbid conditions, such as attention deficit hyperactivity disorder (ADHD), obsessive-compulsive disorder (OCD), school problems, depression, and anxiety [2], leading to its heterogeneous clinical expression [3]. Currently, TS diagnosis is largely depends on the qualitative description of symptoms as there is no hallmark imaging abnormality in routine examination or other reliable diagnostic biomarker [2].

The pathophysiological mechanism that produces tics remains elusive. However, previous neuro-pathological and neuroimaging studies have reported dysfunction of cortico-basal ganglia circuits in relation to tic generation. Exactly,

[a] These authors contributed equally to this work. [*] Correspondence to:
Huiguang He: Research Center for Brain-inspired Intelligence, Institute of Automation, Chinese Academy of Sciences, Beijing, 100190, China. E-mail: huiguang.he@ia.ac.cn
Yun Peng: Department of Radiology, Beijing Children's Hospital, Capital Medical University. No.56 Nanlishi Road, West District, Beijing, 100045, China. E-mail: ppengyun@yahoo.com

Medical Imaging 2017: Biomedical Applications in Molecular, Structural, and Functional Imaging
edited by Andrzej Krol, Barjor Gimi, Proc. of SPIE Vol. 10137, 101371E · © 2017 SPIE
CCC code: 1605-7422/17/$18 · doi: 10.1117/12.2254093

cortical structural changes were found in prefrontal, sensori-motor, anterior cingulate, parietal and temporal regions [4-7], with altered volumes of the corpus callosum [8], basal ganglia [9] and thalamus [10] were also been found. Apart from the macroscopic volumetric changes, several studies pointed to spread microstructural abnormalities in white matter (WM) extend beyond motor pathways in TS patients [11, 12]. However, these studies only revealed TS related structural alterations in some individual brain regions or pathways. As the human brain is a complex network of structurally and functionally interconnected regions, therefore, it is meaningful to study TS related neurological disorders from a network perspective. The brain structural networks [13] could provide us with an anatomical and physiological substrate of brain functions and helps us to understand how the brain structures shape functional interactions [14]. The previous studies investigating the brain's underlying network structure are motivated by the idea that brain function is not solely attributable to individual regions and connections, but rather emerges from the topology of the network as a whole, the human connectome [15].

Previous structural brain network studies have demonstrated that the existence of highly connected brain regions and their efficient interconnections are two important network attributes that jointly promote integrative information processing and adaptive behavior [15, 16]. Those highly interconnected hubs tend to connect to one another has been termed the 'rich club', defined as a set of nodes maintaining a large number of connections, which tends to form strongly interconnected clubs within brain networks. In human network studies, rich club nodes were demonstrated to form an anatomical infrastructure for highly valuable communication between functional resting-state networks (RSNs) [17], and rich club organization is a common feature of power grids and transportation systems, which likely allows for maximal integration and resilience to local disruptions [18]. Despite recent structural brain studies using diffusion tensor imaging (DTI) methods pointed to widespread inter-regional structural connectivity (SC) abnormalities in TS [19, 20], however, it remains unclear whether or not altered organizations of SC networks in TS patients have a selective disruption disproportionally involving rich club regions-related connections.

Considering the unique position of the topologically central role of densely interconnected brain hubs, namely the rich club nodes, have a key role in the global topology of the brain's network. Therefore, in this study, we used diffusion tractography and graph theory analysis to reveal the rich-club organization of SC networks. We investigated whether the altered SC of hubs constitutes a nonspecific generalized phenomenon involving WM connectivity to and from all brain regions, and whether this disruption disproportionally involves pathways that link highly connected regions. We tested the hypothesis that disturbed wiring of this central rich club may contribute to the pathophysiology of TS.

2. MATERIALS AND METHODS

2.1 Subjects

44 TS patients were recruited from outpatient clinics in Beijing Hospital from July 2012 to May 2015 (age: 8.98±3.114 years, range: 3–16 years; 11 female). All the patients were drug-naive subjects to exclude the effects of stimulants, as previous studies have suggested that stimulants can significantly influence the structure and function of central nervous system in TS [21]. All the patients met DSM-IV-TR (Diagnostic and Statistical Manual of Mental Disorders, 4th Edition, text revision) criteria for TS. We also included 48 healthy children in our study (age: 11.00±3.495 years; range: 3–17 years; 17 female). We used a clinical interview and the Children's Yale-Brown Obsessive Compulsive Scale (CY-BOCS) [22] to diagnose OCD and used the German short version of Wender Utah rating scale (WURS-k, translated to Chinese) [23] to diagnose ADHD. Patients fulfilling OCD criteria or other co-morbidities were excluded from the study. As a previous TS classification study [24] tested specifically for differences between TS children with and without ADHD, and found no significant differences in individual accuracy or in the proportion of children classified correctly. Based on similar consideration, in this study, we included children with ADHD as our previous studies [19, 25]. Tic severity for all patients was rated using the Yale Global Tic Severity Scale (YGTSS) and ranged from 10 to 79 ([mean±SD]: 46.50±18.037). The duration of TS ranged from 3 month to 5 years ([mean±SD]: 1.81±1.423 years). For subjects who had course less than 1 year, TS diagnosis was made by follow-up call and they were all finally diagnosed exactly as TS by our professional neurologists and psychiatrists. After the study was approved by Beijing Children's Hospital review board, written informed consent was obtained from all the parents/guardians according to the Declaration of Helsinki.

2.2 Data acquisition

Magnetic resonance imaging was acquired using a 3.0T MR scanner (Gyroscan Interna Nova, Philips, Netherland). Head positioning was standardized using canthomeatal landmarks. The head was stabilized with foam pads to minimize head movements. Patients were instructed to suppress tics and minimize head movements during scanning as much as possible. Axial three-dimensional diffusion weighted scans were acquired using the following protocol: spin-echo diffusion-weighted echo-planar imaging sequence of 30 non-collinear directions with a b value of 1000 s/mm^2, 2mm slice thickness, no inter-slice gap, repetition time = 4300ms, echo time = 95ms, field of view (FOV) =255×255mm, reconstructed image matrix = 336×336. 3D T1-weighted imaging were performed with axial three-dimensional-Fast Field Echo (3D FFE) sequence with the following parameters: repetition time (TR) = 25ms, echo time (TE) = 4.6ms, flip angle = 30°, reconstructed image matrix = 256×256, field of view (FOV) = 200×200mm, slice thickness = 1mm.

2.3 Data preprocessing

Following data acquisition, all of the 3D T1-weighted images were reoriented with the origin set close to the anterior commissure (AC). We used the FMRIB's Diffusion Toolbox (FDT2.0) within FSL v4.1 (http://www.fmrib.ox.ac.uk/fsl) for DTI processing. For each participant, 30 DTI volumes with 1000s/mm^2 b-value were first affinely registered to the b_0 volume for correction of eddy current distortion and simple head motion. Non-brain voxels were removed using Brain Extraction Tool (BET) of FSL; a fractional intensity threshold of 0.25 was selected, resulting in a brain-extracted 4D image and a binary brain mask for each subject. We then used the eddy-corrected 4D data and corresponding brain mask to fit the diffusion tensor model at each voxel by using the FDT. Eigenvalues of diffusion tensor matrix (λ_1, λ_2, λ_3) were obtained and maps of axial diffusivity (AD=λ_1), mean diffusivity (MD=(λ_1+λ_2+λ_3)/3), and fractional anisotropy (FA) were generated. Radial diffusivity (perpendicular eigenvalue, λ_{23}= (λ_2+λ_3)/2) was calculated by averaging λ_2 and λ_3 maps.

2.4 Brain structural network construction

The whole brain fiber bundles linked different cortical regions form a huge complicated network. The most basic element network nodes and edges are defined as follows.

Network node definition: Briefly, individual T1-weighted images were coregistered to the b0 images in the DTI space. Then, the transformed T1 images were then nonlinearly transformed to the ICBM152 T1 template in the MNI space. The inverse transformations were used to warp the Automated Anatomical Labeling (AAL) atlas [26] from the MNI space to the DTI native space. Of note, the nearest-neighbor interpolation method was used to preserve discrete labeling values. Using this procedure, we obtained 90 cortical and subcortical regions (45 for each hemisphere), each representing a node of the network (Table 1).

Network edge definition: To define the connections (edges) between the brain regions, we constructed networks using deterministic tractography. The whole brain fiber tracking was performed via the Fiber Assignment by Continuous Tracking (FACT) algorithm by seeding from the center of each voxel, with the FA threshold of 0.2 and tracking turning angular threshold of 35°. For every pair of brain nodes/regions defined above, fibers with two end-points located in their respective masks were considered to link the two nodes. We defined the number of connected fibers between two regions as the weights of the network edges. To reduce the risk of false-positive connections due to noise or the limitations in the deterministic tractography, and simultaneously ensured the size of the largest connected component (i.e., 90) in the networks was observed across all subjects, we chose the same threshold (T = 3) as previous studies [27, 28] and the weights below threshold were set to 0.

2.5 Rich club organization

Graph theory analysis was then used to reveal the rich club organization of the structural network. The rich club phenomenon in networks is said to be present when the highly connected (high-degree) hubs of a network are more densely connected among themselves than predicted on the basis of their high degree alone [29]. To identify rich club organization, the number of connections among high-degree nodes is compared to the number of connections that would occur by chance alone. As in this study, we considered the fiber number (FN) weighted networks, the weighted version of the rich club behavior incorporates the weights of the edges in the network, examining the level of density between the subset of selected nodes in the network. For all individual weighted networks, firstly all non-zero connections of the

examined weighted network were ranked in respect to their weight, resulting in a vector W^{ranked}. Secondly, the degree of each node was computed as the number of links to other nodes in the network. A subgraph of the original matrix was then constructed for each degree k, from 1 to the maximum k value, in which only nodes with a degree of at least k were included. Then within each k-th subgraph, the number of all links $E_{>k}$ were counted, and the sum of their collective weight $W_{>k}$ were computed. Finally, the weighted rich-club parameter $\Phi^w(k)$ was computed as the ratio between $W_{>k}$ and the sum of the weights of the strongest $E_{>k}$ connections. Formally, $\Phi^w(k)$was given as follows [15]:

$$\phi^w(k) = \frac{W_{>k}}{\sum_{l=1}^{E_{>k}} w_l^{ranked}} \tag{1}$$

Next, we compare and normalize the rich club coefficient to sets of "equivalent" random networks.

For each network, 1000 random networks were computed with equal size and degree distribution. For each random network the rich club coefficient $\phi_{random}^w$was computed over all levels of k, and the $\phi_{random}^w(k)$ was computed as the average rich club coefficient over the 1000 random networks. The normalized rich club coefficient $\phi_{norm}^w(k)$ was computed as Eq. (2), and when it is greater than 1 for a continuous range of k, the network is said to have rich club organization [15]. For convenience, we referred $\phi_{norm}^w(k)$ to Φ^w for the rest of this paper.

$$\phi_{norm}^w(k) = \frac{\phi^w(k)}{\phi_{random}^w(k)} \tag{2}$$

Table 1. Cortical and subcortical regions of interest defined in our study (45 for each hemisphere), each representing a node of the network.

Regions	Abbr.	Regions	Abbr.
Precentral gyrus	**PreCG**	Lingual gyrus	**LING**
Superior frontal gyrus, dorsolateral	**SFGdor**	Superior occipital gyrus	**SOG**
Superior frontal gyrus, orbital part	**ORBsup**	Middle occipital gyrus	**MOG**
Middle frontal gyrus	**MFG**	Inferior occipital gyrus	**IOG**
Middle frontal gyrus orbital part	**ORBmid**	Fusiform gyrus	**FFG**
Inferior frontal gyrus, opercular part	**IFGoperc**	Postcentral gyrus	**PoCG**
Inferior frontal gyrus, triangular part	**IFGtriang**	Superior parietal gyrus	**SPG**
Inferior frontal gyrus, orbital part	**ORBinf**	Inferior parietal, but supramarginal and angular gyri	**IPL**
Rolandic operculum	**ROL**	Supramarginal gyrus	**SMG**
Supplementary motor area	**SMA**	Angular gyrus	**ANG**
Olfactory cortex	**OLF**	Precuneus	**PCUN**
Superior frontal gyrus, medial	**SFGmed**	Paracentral lobule	**PCL**
Superior frontal gyrus, medial orbital	**ORBsupmed**	Caudate nucleus	**CAU**
Gyrus rectus	**REC**	Lenticular nucleus, putamen	**PUT**
Insula	**INS**	Lenticular nucleus, pallidum	**PAL**
Anterior cingulate and paracingulate gyri	**ACG**	Thalamus	**THA**
Median cingulate and paracingulate gyri	**DCG**	Heschl gyrus	**HES**
Posterior cingulate gyrus	**PCG**	Superior temporal gyrus	**STG**
Hippocampus	**HIP**	Temporal pole: superior temporal gyrus	**TPOsup**
Parahippocampal gyrus	**PHG**	Middle temporal gyrus	**MTG**
Amygdala	**AMYG**	Temporal pole: middle temporal gyrus	**TPOmid**
Calcarine fissure and surrounding cortex	**CAL**	Inferior temporal gyrus	**ITG**
Cuneus	**CUN**		

2.6 Group-averaged network and rich club nodes

For both groups, a group-averaged network was computed according to procedures similar to those outlined in [15]. Briefly, for all individual matrices, only connections that were present in at least 50% of the group were selected for averaging. This yielded connectivity matrices for TS and control group that were well-matched in terms of connection density (11.59% and 11.41% respectively). The network density is defined as the fraction of the number of edges in a graph compared to the maximum possible number of edges. Rich club regions as described throughout this paper were selected on the basis of the group-averaged network, set at a rich club level of k>15, as [15].

2.7 Connection classes: rich club, feeder and local connections

On the basis of the categorization of network nodes into rich club and non–rich club regions, edges of the network were classified into 3 distinct classes: rich club connections linking rich club members, feeder connections linking rich club members to non–rich club members, and local connections connecting non–rich club members. Of note, we identified the rich club, feeder and local connections for each individual TS or control subject, respectively. Only if the edge weight was larger than 0, the connection was deemed to be in existence.

2.8 Other graph metrics of structural networks

In this study, we also calculated other network topological attributes based on graph theory analysis, given as below (Table 2 shows the general descriptions):

S_p: network strength (mean degree), E_{glob}: network global efficiency, E_{loc}: network local efficiency, L_p: the shortest path length, C_p: the clustering coefficient, λ: the normalized shortest path length, γ: the normalized clustering coefficient, and σ: the small-worldness.

Table 2. Global and local topological network properties used in the study.

Global network properties	
Network strength S_p	S_p is the strength of the network, which is defined as the mean degree of all the regions in the brain network.
Global Efficiency E_{glob}	E_{glob} is defined as the mean value of all regions' global efficiency.
Local Efficiency E_{loc}	E_{loc} is defined as the mean value of all regions' local efficiency.
Shortest path length L_p	L_p is defined as the length of the path for node i and node j with the shortest length.
Clustering coefficient C_p	C_p was defined as the likelihood of the neighborhoods connecting with each other.
Small-worldness σ	The network with small-worldness is a kind of network with both high clustering coefficient and low shortest path length.

2.9 Statistical analysis

Two-sample t-tests were used to evaluate the between-group differences of normalized rich club coefficient (Φ^w), eight other graph metrics, the density and number of rich club, feeder, and local connections. We also investigated the Pearson relationship between the Φ^w and other common network metrics, as defined in section 2.8. Partial correlations between clinical variables and rich club related parameters (Φ^w, the number, and density of rich club, feeder, and local connections) were also examined, with age and gender as covariates.

3. RESULTS

3.1 Disrupted rich club organization in TS

In this study, we attempted to identify the existence of rich club organization in both TS and control group using the structural networks. We found significant rich club organization in the group-averaged structural networks in both group across several levels of k (from 16 to 23). However, TS group had a significantly ($p<0.05$, FDR [30] correction for multiple comparisons) increased rich club organization for the range k=18 to k=20, indicating a higher level of interconnectivity between hubs in TS. Figure 1 illustrates the group-averaged normalized Φ^w rich club curves of weighted (by number of fibers) networks in both group.

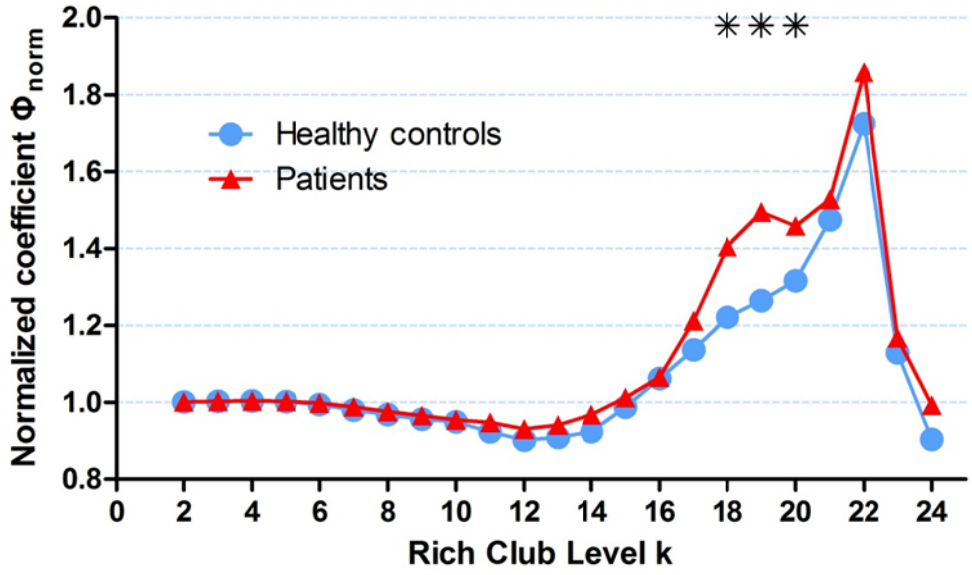

Figure 1. Rich club phenomena in structural group-averaged network of both groups. The normalized rich club coefficient $\Phi_{norm}{}^w$ for controls (blue) and patients (red) were shown. TS patients had a significantly increased rich club coefficient across several levels of k (from 18 to 20). Significant values ($p<0.05$) are signified with an asterisk.

In this study, based on the similar considerations as the previous study [15], rich club regions were selected on the basis of the group-averaged network, set at a rich club level of $k>15$. Of note, in our results, the significant rich club organization began to emerge at a rich club level of $k>15$ in both groups, indicating the rationality of the selection.

The rich club regions in group-averaged network were also found altered between groups. Rich club regions found in both groups included the bilateral precuneus (PCUN), right precentral gyrus (PreCG) and putamen (PUT). The right dorsolateral superior frontal gyrus (SFGdor), left temporal pole of superior temporal gyrus (TPOsup) and PUT were rich club regions only in control group, while the right Insula (INS) and middle temporal gyrus (MTG) were rich club regions only in TS group, indicating the disrupted rich-club organization in TS children (Figure 2).

3.2 Altered number and density of feeder connections

After the rich club regions in group-averaged network were defined in both groups, the rich club, feeder, and local connections of each individual network were decided. We examine the density and number of rich club, feeder, and local connections in the brain structural network for each subject. Statistical testing revealed TS group had significantly ($p<0.05$) increased density and significantly decreased number in feeder connections (Figure 3). In addition, the number of local connections was significantly increased in TS group. In contrast, the between-group differences of density and number were not significant for the rich club connections.

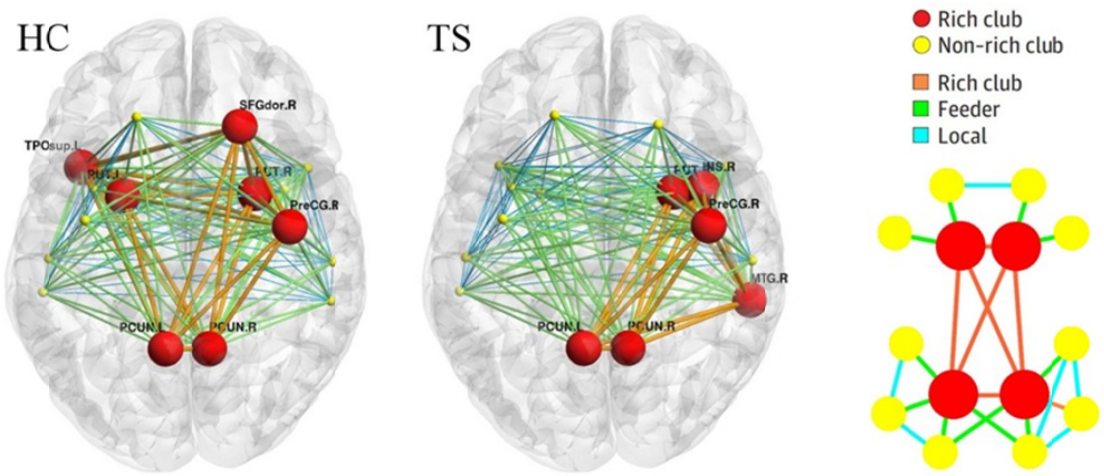

Figure 2. Altered rich club distributed across structural networks between groups. This figure is based on the group-averaged networks (at a rich club level of k >15). Edges across individual brain networks (both controls and patients) were divided into 3 distinct classes: rich club connections linking rich club members (red), feeder connections linking rich club members to non–rich club members (green), and local connections connecting non–rich club members (blue edges). To make the presentation easy, only a fraction of non-rich club were shown.

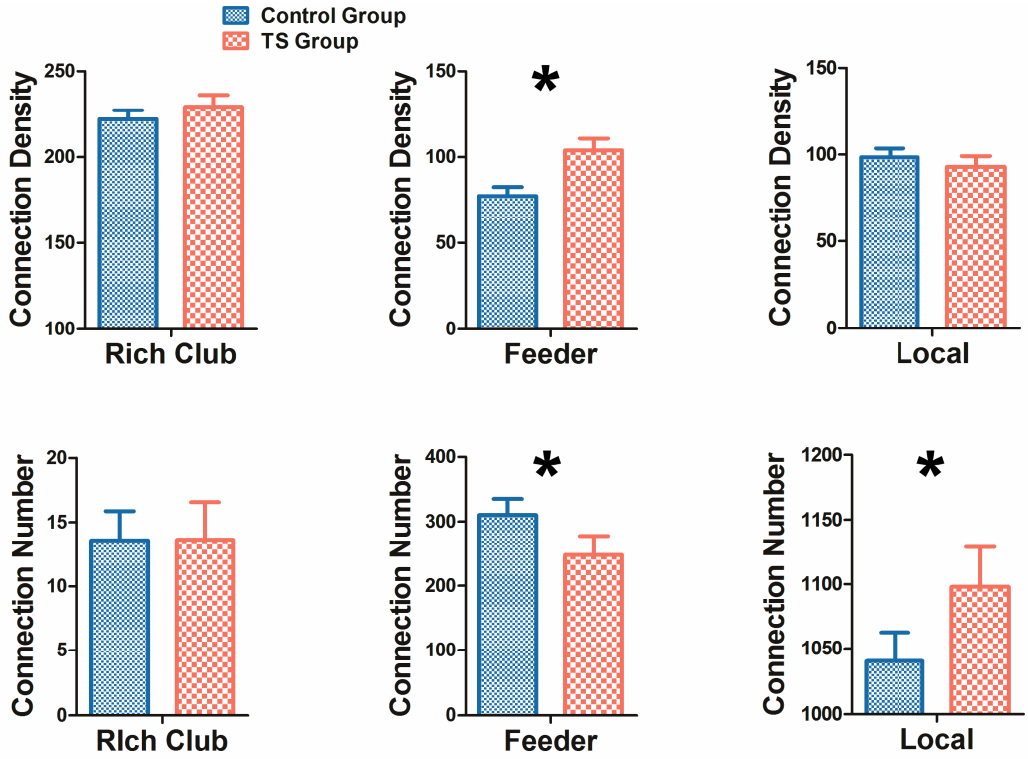

Figure 3. Examining the density of rich club, feeder, and local connections between the populations of controls and patients revealed a significant reduction in rich club density in patients but no significant effect in density of feeder and local connections.

3.3 No significant alteration in other graph metrics

In this study, we also examined eight other graph metrics of structural networks. Both TS patients and controls showed a small-world organization of WM networks characterized by $\gamma>1$ and $\lambda\approx1$. In addition, there were no significant differences between groups in all the eights graph-based network metrics (Table 3).

Table 3. Between-group comparisons of other graph-based network properties.

	S_p	E_{glob}	E_{loc}	L_p	C_p	λ	γ	σ
HC	1430±203	76.37±11.16	117.2±15.6	0.013±0.002	0.020±0.007	1.19±0.40	4.18±0.32	3.52±0.26
TS	1452±292	77.92±15.60	119.4±22.3	0.013±0.003	0.018±0.010	1.18±0.49	4.23±0.30	3.58±0.25
p value	0.680	0.583	0.585	0.927	0.483	0.484	0.450	0.246

Two sample t-tests were used to determine the differences in the graph-based network properties between groups.

3.4 Correlations between rich club coefficient and other graph metrics

For the correlations between Φ^w and other network metrics, in the control group, the γ and small-worldness σ presented the significantly positive correlation with Φ^w, while in the TS group, the C_p and λ presented the significantly negative correlation with Φ^w. There was no significantly correlation for other metrics (Figure 4).

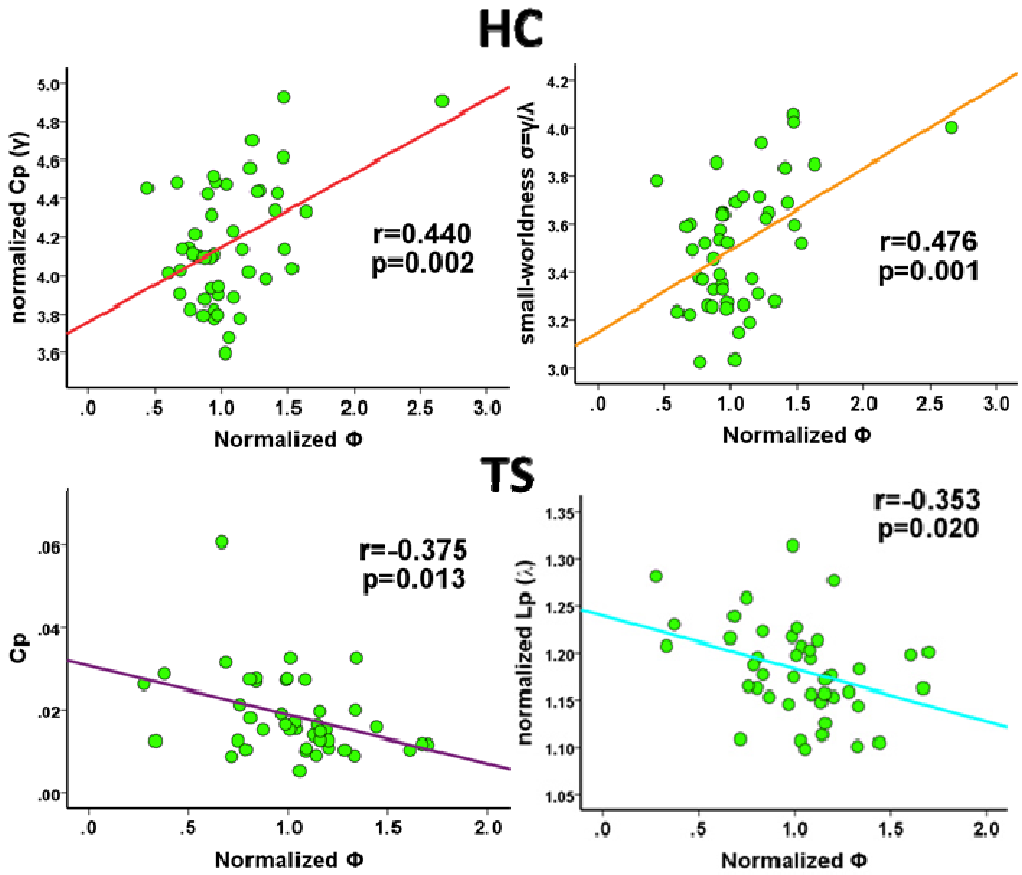

Figure 4. Pearson correlations between the normalized rich club coefficients and other common network metrics. All the results were derived at a rich club level of k>15. HC: healthy controls.

3.5 Correlations between clinical variables and rich club related parameters

To investigate the clinical relevance of the altered brain structural network topologies in TS, we correlated the clinical variables (disease duration, and tic severity score/YGTSS) with the rich club related parameters (Φ^w, the number, and density of rich club, feeder, and local connections). In our results, the YGTSS was significant positively correlated with normalized rich club coefficient ($r = 0.334$, $p = 0.033$) and the number of feeder connections ($r = 0.310$, $p = 0.049$) (Figure 5). No significant correlations were found in other clinical variables and rich club related parameters.

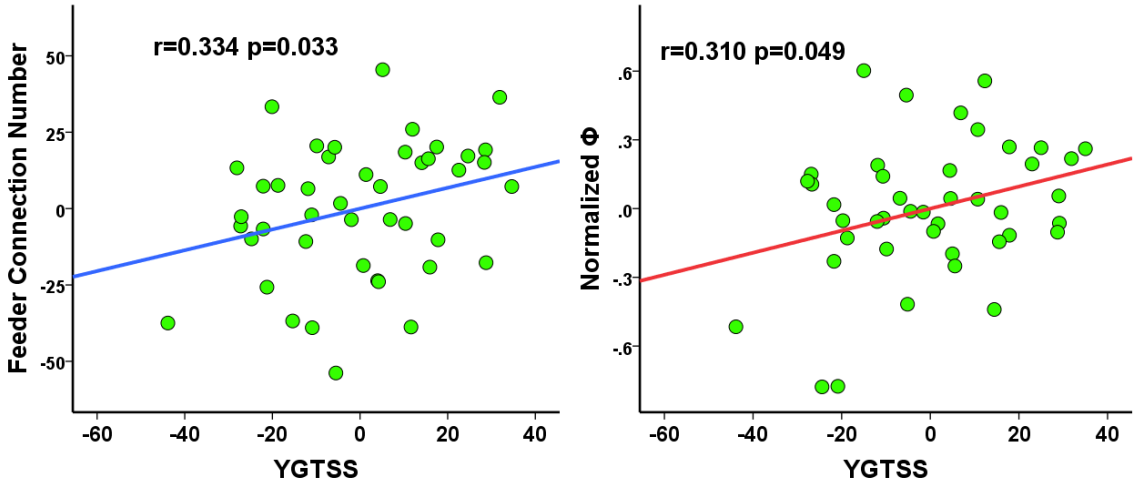

Figure 5. Correlations between rich club related metrics and clinical variables. YGTSS shows significantly positive correlations with normalized rich club coefficient and the number of feeder connections. Of note, the X-axis and Y-axis only reflect the partial correlation of network metric and YGTSS, while considering age and gender as covariables.

4. DISCUSSION

At present, the topological disruptions of the whole brain WM structural networks, especially the rich club organization, which may underlie functional or structural abnormalities in TS, remain poorly understood. In the present study, we aimed to take a critical step toward this goal, and applied graph theoretical methods to neuroimaging studies, in order to explore questions about large scale system organization that were previously difficult to attain. We used both diffusion tractography and graph theory analysis to explore the structural rich club organization from multiple levels.

4.1 An increased level of rich club interconnectivity in TS

In this study, we revealed TS group had a significantly increased normalized rich club coefficient across several levels of degree, indicating an increased level of rich club interconnectivity in TS children. The connections among rich club brain hubs have been proposed to be central to the integration of information among different subsystems of the human brain [31]. Therefore, our findings suggest that TS is characterized by increased structural integrity of this centrally embedded rich club backbone, potentially resulting in increased global communication capacity and altered functional brain dynamics.

4.2 The reorganization of rich club regions in TS

Our study suggests that altered SC in brain network, in particular the reorganization of rich club regions, is related to pathology of TS. Compared to controls, the main altered rich club regions in TS children were in the right insula, middle temporal gyrus, dorsolateral superior frontal gyrus, left temporal pole of superior temporal gyrus and putamen, which were reported to be highly related to TS [19, 25, 27, 32]. Previous structural network studies in TS [20] have

shown altered structural connectivity in cortico-striato-pallido-thalamic networks. Extending previous findings, this study now reveals disrupted rich club connectivity on a global scale in early TS children.

4.3 Rich club organization related to other graph metrics

In our results, the tight correlations between the normalized rich club coefficients and the normalized clustering coefficient, small-worldness exist in healthy children were disrupted in TS group, indicating if the hubs were attacked, the robustness of small-world topology and efficiency of the network would be obviously compromised. The clustering coefficient represents the ability of a network to process specialized information within densely interconnected groups of nodes (functional segregation), while networks which have a relatively high rich-club coefficient are said to demonstrate the rich-club effect and will have many connections between nodes of high degree. Therefore, our findings indicated that the increased level of rich club connectivity would cause higher clustering coefficient in TS patients (compared to random networks), thereby SC networks in TS are more likely to be connected to each other, thereby indicating that they are more synchronized, segregated and less independent of each other.

4.4 Increased feeder connections density highly related to pathology of TS

Intriguingly, in this study, we also found TS group had significantly increased density and significantly decreased number in feeder connections. Moreover, the increased feeder connections density of TS children were significantly positively correlated to tic severity, indicating a close association between tic severity and a disturbance in structural connections between rich club regions and non-rich club regions. In the healthy brain, while rich club connections form a backbone for efficient, high-capacity global brain network communication [15, 31], feeder connections carrying heavier network traffic provide communication with important nodes, which is also crucial for managing global network information transmission. As the topologically central role of rich club regions and their related brain connections are highly vulnerable to pathological brain lesions [33], our findings suggested that TS may be characterized by increased structural integrity between rich club regions and non-rich club regions. Furthermore, the positive correlation between the tic severity and the level of feeder connectivity density further suggested that the risk of structural connectivity alteration between rich club and non-rich club regions increased with greater tic severity, hence more aggressive treatment of TS could be indicated.

5. CONCLUSION

The main finding of this study is an increased level of rich club interconnectivity in WM structural networks of TS children. The rich club regions in group-averaged structural network were also found altered in TS. In addition, the number and density of feeder and local connections were found to be significantly affected in TS group, indicative of TS to be associated with a disturbance in structural connectivity among key hubs of the human brain. The rich club takes a central position in the brain's network topology and feeder connections have been proposed to connect more remote nodes with a route or branch carrying heavier traffic, which is crucial for. Our findings suggest that TS is characterized by increased structural integrity of this centrally embedded rich club backbone, potentially resulting in increased global communication capacity and altered functional brain dynamics. Our findings may provide structural insights into the brain networks of TS children and help reveal the pathological mechanism of TS.

ACKNOWLEDGEMENTS

We thank Dr. Hao Huang at University of Pennsylvania for consultation and support on MR pulse sequences

This work was supported by National Natural Science Foundation of China (91520202, 61271151, 31271161), Youth Innovation Promotion Association CAS and Beijing Municipal Administration of Hospitals Incubating Program (PX2016035), Beijing health system top level health technical personnel training plan (2015-3-082).

AUTHOR CONTRIBUTIONS

Designed and performed experiment: Hongwei Wen; Wrote the manuscript and prepared the figures and tables: Hongwei Wen; Conceived and designed the project: Huiguang He, Yun Peng, Yue Liu; Data Collection: Yue Liu, Jishui Zhang; Obtaining funding: Huiguang He, Yun Peng, Yue Liu. All the authors revised and approved the manuscript.

REFERENCES

[1] Liu, Y., Miao, W., Wang, J., Gao, P., Yin, G., Zhang, L., Lv, C., Ji, Z., Yu, T., Sabel, B.A., He, H., Peng, Y.: Structural abnormalities in early Tourette syndrome children: a combined voxel-based morphometry and tract-based spatial statistics study. Plos One 8, e76105 (2013)

[2] Felling, R.J., Singer, H.S.: Neurobiology of tourette syndrome: current status and need for further investigation. Journal of Neuroscience the Official Journal of the Society for Neuroscience 31, 12387-12395 (2011)

[3] Cavanna, A.E., Servo, S., Monaco, F., Robertson, M.M.: The behavioral spectrum of Gilles de la Tourette syndrome. The Journal of neuropsychiatry and clinical neurosciences 21, 13-23 (2009)

[4] Peterson, B.S., Staib, L., Scahill, L., Zhang, H., Anderson, C., Leckman, J.F., Cohen, D.J., Gore, J.C., Albert, J., Webster, R.: Regional brain and ventricular volumes in Tourette syndrome. Archives of general psychiatry 58, 427-440 (2001)

[5] Sowell, E., Kan, E., J, Thompson, P., Bansal, R., Xu, D., Toga, A., Peterson, B.: Thinning of sensorimotor cortices in children with Tourette syndrome. Nat Neurosci 11, 637-639 (2008)

[6] Muller-Vahl, K.R., Kaufmann, J., Grosskreutz, J., Dengler, R., Emrich, H.M., Peschel, T.: Prefrontal and anterior cingulate cortex abnormalities in Tourette Syndrome: evidence from voxel-based morphometry and magnetization transfer imaging. Bmc Neurosci 10, (2009)

[7] Cherine, F., Uicheul, Y., Samir, D., Oliver, L., John, C., Rozie, A., Guy, R., Paul, S., Kirk, F., Catherine, B.: Somatosensory-motor bodily representation cortical thinning in Tourette: effects of tic severity, age and gender. Cortex; a journal devoted to the study of the nervous system and behavior 46, 750-760 (2010)

[8] Plessen, K.J., Wentzel-Larsen, T., Hugdahl, K., Feineigle, P., Klein, J., Staib, L.H., Leckman, J.F., Bansal, R., Peterson, B.S.: Altered interhemispheric connectivity in individuals with Tourette's disorder. Am J Psychiat 161, 2028-2037 (2004)

[9] Peterson, B.S., Thomas, P., Kane, M.J., Scahill, L., Zhang, H.P., Bronen, R., King, R.A., Leckman, J.F., Staib, L.: Basal ganglia volumes in patients with Gilles de la Tourette syndrome. Archives of general psychiatry 60, 415-424 (2003)

[10] Miller, A.M., Ravi, B., Xuejun, H., Juan Pablo, S.P., Sobel, L.J., Jun, L., Dongrong, X., Hongtu, Z., M Mallar, C., Kathleen, D.: Enlargement of thalamic nuclei in Tourette syndrome. Archives of general psychiatry 67, 955 (2010)

[11] Neuner, I., Kupriyanova, Y., Stocker, T., Huang, R., Posnansky, O., Schneider, F., Tittgemeyer, M., Shah, N.J.: White-matter abnormalities in Tourette syndrome extend beyond motor pathways. Neuroimage 51, 1184-1193 (2010)

[12] Neuner, I., Kupriyanova, Y., Stocker, T., Huang, R.W., Posnansky, O., Schneider, F., Shah, N.J.: Microstructure assessment of grey matter nuclei in adult tourette patients by diffusion tensor imaging. Neuroscience letters 487, 22-26 (2011)

[13] Sporns, O., Tononi, G., Kotter, R.: The human connectome: A structural description of the human brain. PLoS computational biology 1, e42 (2005)

[14] Qi, S., Meesters, S., Nicolay, K., Bm, T.H.R., Ossenblok, P.: Structural Brain Network: What is the Effect of LiFE Optimization of Whole Brain Tractography? Frontiers in Computational Neuroscience 10, (2016)

[15] van den Heuvel, M.P., Sporns, O.: Rich-club organization of the human connectome. J Neurosci 31, 15775-15786 (2011)

[16] Heuvel, M.P.V.D.: High-cost, high-capacity backbone for global brain communication. Proceedings of the National Academy of Sciences 109, 11372-11377 (2012)

[17] Li, K., Liu, L., Yin, Q., Dun, W., Xu, X., Liu, J., Zhang, M.: Abnormal rich club organization and impaired correlation between structural and functional connectivity in migraine sufferers. Brain Imaging & Behavior 1-15 (2016)

[18] Grayson, D.S., Al, E.: Structural and Functional Rich Club Organization of the Brain in Children and Adults. Plos One 9, e88297-e88297 (2014)
[19] Wen, H., Liu, Y., Wang, J., Rekik, I., Zhang, J., Zhang, Y., Tian, H., Peng, Y., He, H.: Combining tract- and atlas-based analysis reveals microstructural abnormalities in early Tourette syndrome children. Human brain mapping 37, 1903-1919 (2016)
[20] Worbe, Y., Marrakchi-Kacem, L., Lecomte, S., Valabregue, R., Poupon, F., Guevara, P., Tucholka, A., Mangin, J.F., Vidailhet, M., Lehericy, S., Hartmann, A., Poupon, C.: Altered structural connectivity of cortico-striato-pallido-thalamic networks in Gilles de la Tourette syndrome. Brain 138, 472-482 (2015)
[21] Golden, G.S.: The effect of central nervous system stimulants on Tourette syndrome. Ann Neurol 2, 69–70 (1977)
[22] Scahill, L., Riddle, M.A., McSwiggin-Hardin, M., Ort, S.I., King, R.A., Goodman, W.K., Cicchetti, D., Leckman, J.F.: Children's Yale-Brown Obsessive Compulsive Scale: reliability and validity. J Am Acad Child Adolesc Psychiatry 36, 844-852 (1997)
[23] Retz-Junginger, P., Retz, W., Blocher, D., Stieglitz, R.D., Georg, T., Supprian, T., Wender, P.H., Rosler, M.: [Reliability and validity of the Wender-Utah-Rating-Scale short form. Retrospective assessment of symptoms for attention deficit/hyperactivity disorder]. Der Nervenarzt 74, 987-993 (2003)
[24] Greene, D.J., Church, J.A., Dosenbach, N.U.F., Nielsen, A.N., Adeyemo, B., Nardos, B., Petersen, S.E., Black, K.J., Schlaggar, B.L.: Multivariate pattern classification of pediatric Tourette syndrome using functional connectivity MRI. Developmental Science 19, 581–598 (2016)
[25] Wen, H., Liu, Y., Rekik, I., Wang, S., Chen, Z., Zhang, J., Zhang, Y., Peng, Y., He, H.: Multi-modal multiple kernel learning for accurate identification of Tourette syndrome children. Pattern Recognition 63, 601-611 (2017)
[26] Tzourio-Mazoyer, N., Landeau, B., Papathanassiou, D., Crivello, F., Etard, O., Delcroix, N., Mazoyer, B., Joliot, M.: Automated Anatomical Labeling of Activations in SPM Using a Macroscopic Anatomical Parcellation of the MNI MRI Single-Subject Brain. Neuroimage 15, 273-289 (2002)
[27] Wen, H., Liu, Y., Wang, J., Zhang, J., Peng, Y., He, H.: A diagnosis model for early Tourette syndrome children based on brain structural network characteristics. In: SPIE Medical Imaging, pp. 97852R-97852R-97859. International Society for Optics and Photonics, (2016)
[28] Liu, Y., Duan, Y.Y., He, Y., Wang, J., Xia, M.R., Yu, C.S., Dong, H.Q., Ye, J., Butzkueven, H., Li, K.C., Shu, N.: Altered Topological Organization Of White Matter Structural Networks In Patients With Neuromyelitis Optica. Mult Scler J 19, 666-667 (2013)
[29] van den Heuvel, M.P., Sporns, O., Collin, G., Scheewe, T., Mandl, R.C., Cahn, W., Goni, J., Hulshoff Pol, H.E., Kahn, R.S.: Abnormal rich club organization and functional brain dynamics in schizophrenia. JAMA psychiatry 70, 783-792 (2013)
[30] Benjamini, Y., Hochberg, Y.: Controlling The False Discovery Rate - A Practical And Powerful Approach To Multiple Testing. Journal of the Royal Statistical Society 57, 289-300 (2015)
[31] van den Heuvel, M.P., Kahn, R.S., Goni, J., Sporns, O.: High-cost, high-capacity backbone for global brain communication. Proc Natl Acad Sci U S A 109, 11372-11377 (2012)
[32] Wen, H., Liu, Y., Wang, J., Zhang, J., Peng, Y., He, H.: Using support vector machines with tract-based spatial statistics for automated classification of Tourette syndrome children. In: SPIE Medical Imaging, pp. 97852Q-97852Q-97859. International Society for Optics and Photonics, (2016)
[33] Crossley, N.A., AndreaMechelli, JessicaScott, FrancescoCarletti, Fox, P.T., PhilipMcGuire, Bullmore, E.T.: The hubs of the human connectome are generally implicated in the anatomy of brain disorders. Brain 137, 2382-2395 (2014)